Wireless Optogenetic Neural Dust for Deep Brain Stimulation

Stefanus A. Wirdatmadja*, Sasitharan Balasubramaniam*, Yevgeni Koucheryavy*, Josep Miquel Jornet†
*Department of Electrical Engineering and Communications
Tampere University of Technology, Finland
Email: (stefanus.wirdatmadja, sasi.bala, yk)@tut.fi
†Department of Electrical Engineering
University at Buffalo, The State University of New York
Buffalo, NY, 14260
Email: jmjornet@buffalo.edu

***Abstract*—In recent years, numerous research efforts have been dedicated towards developing efficient implantable devices for Deep Brain Stimulation (DBS). However, there are limitations and challenges with the current technologies. Firstly, the stimulation of neurons currently is only possible through implantable electrodes which target a population of neurons. This results in challenges in the event that stimulation at the single neuron level is required. Secondly, a major hurdle still lies in developing miniature devices that can last for a lifetime in the patient's brain. Recently, the concept of neural dust has been introduced as a way to achieve single neuron monitoring and potentially actuation. In parallel to this, the field of optogenetics has emerged where the aim is to stimulate neurons using light, usually by means of optical fibers inserted through the skull. Obviously, this introduces many challenges in terms of user friendliness and biocompatibility. We address this shortcoming by proposing the wireless optogenetic neural dust (*wi-opt neural dust*). The wi-opt neural dust is equipped with a miniature LED that is able to stimulate the genetically engineered neurons, and at the same time harvest energy from ultrasonic vibrations. The simulation results presented in the paper investigates the behaviour of the light propagation in the brain tissue, as well as the performance of designed circuitry for the energy harvesting process. The results demonstrates the feasibility of utilizing wi-opt neural dust for long term implantation in the brain, and a new direction towards precise stimulation of neurons in the cortex.**

I. Introduction

In recent years numerous neurological disorders have led researchers to seek new solutions to improve monitoring as well as treatment techniques. For example, solutions have been developed for electrodes to be placed into the brain and upon stimulation will lead to minimisation of trembling due to parkinson disease. In another work, known as *optogenetics*, optical light is used to stimulate genetically engineered neurons that are sensitive to light at a particular wavelength [1]. The use of optogenetics can lead to precise single neuron stimulation. However, a major drawback with the current techniques is the fact that the technologies require insertion of electrodes or optical cables into the skull. While it does solve the problems, and opens up innovation, the proposed techniques are not practical for everyday use by the patients.

In this paper, we propose the *wireless optogenetics neural dust*, which we refer to as *wi-opt neural dust*. The wi-opt neural dust advances the neural dust proposed by [2], which is only limited to monitoring the neurons and reporting back to the *sub-dura transceiver* through back scattering. The benefits of integrating the wireless optogenetic component to the neural dust is to enable single neuron stimulation, while envisioning long term implantation of the device. However, there are a number of challenges in realising a fully operational wi-opt neural dust. Firstly, the devices will need to be powered, and this is a challenge given the miniature size of the entire unit. For practical use, the device must avoid the use of batteries, which could potentially lead to toxic leaks as well as requirements of surgery to change them. Secondly, since our objective is to stimulate the neurons, the energy harvesting component is required to absorb sufficient amount of energy that can be used for stimulation. The paper addresses each of these challenges by proposing a design of the device that is able to harvest energy from ultrasound waves, which is used to power a LED unit. The paper presents simulation work to demonstrate the feasibility of the wi-opt neural dust, by initially presenting the behaviour of the light propagation in the brain tissue based on the energy harvested, as well as the energy harvesting efficiency based on variations of the ultrasonic frequency, as well as size and components of the wi-opt neural dust circuitry.

This paper is organized as follows: Sec. II introduces the system model of the wi-opt neural dust. Sec. III presents the circuitry of the device, while the simulation of the wi-opt neural device is discussed in Sec. IV. Lastly, Sec. V presents the conclusion.

II. System Model

The neural dust architecture, first introduced in [2] is illustrated in Fig. 1. It will be the same proposed in this paper. The architecture consist of wi-opt neural dust devices that are embedded in various parts of the cortex and interfaces to neurons.

Unlike the neural dust, the wi-opt neural dust contains a LED that interfaces to neurons and stimulates it using light, as illustrated in Fig. 2. The neurons in this case are engineered to be sensitive to light at a specific wavelength

978-1-5090-3370-6/16/$31.00 ©2016 IEEE

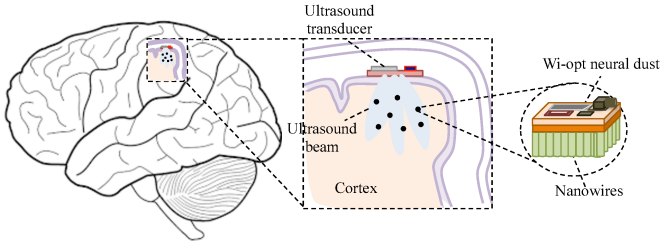

Fig. 1. Illustration of the ultrasound wi-opt neural dust network, which are scattered in the various layers of the cortex. The sub-dura transceiver is used to emit ultrasound signals to charge and trigger the wi-opt neural dust for deep brain stimulation.

Fig. 2. Illustration of an wi-opt neural dust that interfaces to an engineered neuron that is sensitive to light at a specific wavelength.

(in our case, this will be at 470nm). Above the cortex is the *sub-dura transceiver* that communicates with the wi-opt neural dust using ultrasonic signals. The purpose of the ultrasound communication to the device is two fold: ultrasonic waves are both used to instruct the device to stimulate the neuron and to provide the required energy. The sub-dura transceiver acts as a middle-man device that in turn communicates with the external transceiver. Therefore, the entire architecture consists of three layers of communication. In this paper, we only limit the interaction between the sub-dura transceiver and the wi-opt neural dust devices.

The cortex is composed of gray matter where the neural cell bodies and glial cells are the major population. The neurons are grouped into six vertical stacked layers with different cell types, such as: *pyramidal cells*, *spiny stellate cells*, *basket cells*, *chandelier cells*, and *smooth stellate cells* [3]. The total thickness of the cortex is approximately 2-6 mm, and it is within this region that the wi-opt neural dusts will be scattered. In addition to vertical scattering, the wi-opt neural dust can also be horizontally scattered, where each layer will have the devices scattered at different densities. The average human brain length and width is approximately 167 mm and 140 mm. Therefore, the wi-opt neural dusts should have certain coverage to operate properly considering the attenuation due to brain tissue absorption of the ultrasound, as well as the number of damaged neurons that are required to be stimulated.

III. Wireless Optogenetic Neural Dust

Fig. 3 illustrates the circuit diagram of the wi-opt neural dust. The energy harvester of the wi-opt neural dust contains

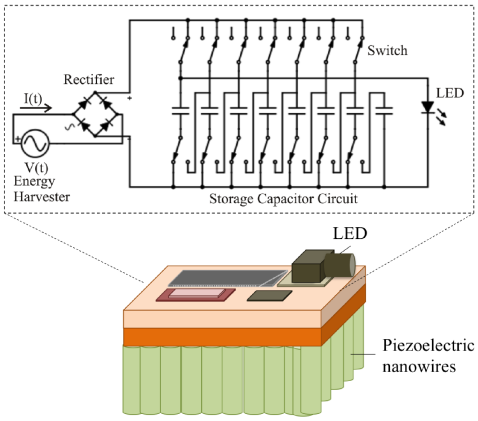

Fig. 3. Device architecture of the wi-opt neural dust, including the internal circuit diagram.

piezoelectric nanowires that that vibrate because of the ultrasounds, and through a transducer converts the mechanical energy to electrical energy. The power intensity of the ultrasound wave source is regulated by the Food and Drug Administration (FDA), where the safety level limit is $720 mW/cm^2$. Since the current generated from the piezoelectric nanowire is in AC, the conversion to DC is achieved through a rectifier. The DC current is then be charged through a series of capacitors which stores the required energy for powering the LED. The circuit also contains a switch that passes the current to the LED, and this is also sensitive to specific frequency of the ultrasound waves (this is the inherent addressing mechanism of each of the devices)

A. Energy Harvester

There are a wide range of available piezoelectric materials, and these include *lead zirconate titanate* (*PZT*), *aluminum nitride* (*AlN*), *barium titanate* (*BaTiO3*), and *zinc oxide* (*ZnO*) in the form of crystal or nanowires [4] [2] [5]. The energy harvester used in this paper is based on the ZnO nanowires with thin coating to eliminate any negative effect on the brain tissue. An example coating that could be used is based on the works of [4] that used a thin layer (<100 μm) of acrylic *Polymethyl methacrylate*) coating. Experiments have also shown that the coating did not exhibit any significant performance degradation on the energy harvesting process. One important component required in energy harvesting applications is the electromechanical coupling coefficient. This parameter defines the conversion efficiency between mechanical and electrical energy. It is affected by the geometry structure of the material [6].

The generated ultrasound wave traverses through the brain tissue whose attenuation coefficient α is 0.435 dB/(cm·MHz) [7]. As a result, the power intensity level received by the wi-opt neural dust is less due to the attenuation according to the following equation:

$$P_{nd} = P_s \exp^{-(\alpha f d/10)}, \quad (1)$$

where P_{nd} and P_s are the power intensity level at the surface of the device and the acoustic wave source, respectively, α is the attenuation coefficient of the brain tissue, f is the acoustic wave frequency, and d is the distance between the wi-opt neural dust and the sub-dura transceiver. Due to this factor, 720 mW/cm^2 acoustic wave radiation is attenuated to $\approx 60mW$ on a $100 \times 100\mu m^2$ wi-opt neural dust mote implanted at 2 mm brain tissue of the cortex. Moreover, not all the acoustic wave power received by the neural dust mote is converted to electrical power, and this depends on the conversion rate of the corresponding energy harvester. Suppose that the conversion rate (η) is 0.5, the electrical power generated by it is 30 mW. The conversion process is represented as

$$P_{nd} = i_{nd} A_{EH}, \tag{2}$$

$$P_e = P_{nd}\eta, \tag{3}$$

where P_{nd} and P_e are the power received to vibrate the nanowire energy harvester and the electrical power after the conversion from mechanical to electrical energy; A_{EH} is the effective surface area of the energy harvester.

B. Storage Capacitors

As the nanowires generates AC current, full-wave rectification is required before the generated signal is fed to the capacitors. Since the generated voltage from nanowires (V_g) is 0.42 V [8], several capacitors are required to fulfill the energy requirement of the LED. For this purpose, micro-supercapacitors based on interdigital electrodes of reduced graphene oxide and carbon nanotube composite can be used [9]. Based on the electrical power and voltage supplied by energy harvester, the flowing current (I_g) can be represented as:

$$I_g = \frac{P_e}{V_g}. \tag{4}$$

A single micro-supercapacitor with the surface area of 100 x 100 μm^2 has a capacitance value of 280 μF. Due to the limited voltage source and power requirements of the LED, different capacitor circuits are required during the charging and discharging cycles. A parallel capacitor circuit is used during the charging process, while a series connection is used for the discharging process. For a single supercapacitor C_{cap}, the number of different capacitance value n for the series $C_{cap_{ser}}$ and parallel $C_{cap_{par}}$ connections can be represented as:

$$C_{cap_{par}} = nC_{cap}, \tag{5a}$$

$$C_{cap_{ser}} = \frac{C_{cap}}{n}. \tag{5b}$$

Therefore, the total voltage fed to the LED is the sum of the voltage of the n capacitors. Depending on the vibration frequency of the nanowires, the electrical charging rate can be formulated as [8]:

$$\Delta Q = I_g t_{cycle} = \frac{I_g}{freq}, \tag{6}$$

where ΔQ is the electrical charge per cycle, I_g is the current from the energy harvester, and $t_{cycle} = \frac{1}{freq}$ is the cycle period for the emitted ultrasound waves.

C. Light Source and Optogenetics

In optogenetics, the neurons are genetically engineered so that the ion channels are sensitive to light at a specific wavelength. Upon illumination of light, the neuron generates Action Potential (AP) which in turn triggers an electro-chemical signal along the axon of the cell. One approach of engineering the cell is to use *Channelrhodopsin-2* (*ChR2*) which is a protein extracted from green alga *Chlamydomonas reinhardtii* that modifies the cells to have light-gated cation-selective membrane channels [10].

In order to model the circuit to excite the optogenetic process, the light intensity level should be at an optimum level. The excitation needs to be low enough to utilize the limited electrical energy and sufficiently high to satisfy the power requirements of the LED. The optogenetic construct *ChR2* gets activated by $\approx$ 470 nm light with an intensity of $\approx$ 1 mW/mm^2 [11]. For the LED unit, the InGaN Cree's Direct Attach DA2432 LED [12] can be used in this application. This LED can operate with an electrical current level starting from 5 mA with wave length of 465 nm that generates $\approx$ 5 mW of optical power [13].

Inside the brain tissue, light wave experiences scattering, absorption, and conical (geometrical) spreading. This effect can be formulated by the *Kubelka-Munk* model which gives the theoretical calculation for light propagation through scattering and absorptive media [14].

$$\frac{I(z)}{I(z=0)} = \frac{\rho^2}{(Sz+1)(z+\rho)^2}, \tag{7}$$

$$\rho = r\sqrt{\left(\frac{n}{NA}\right)^2 + 1}, \tag{8}$$

where r is the radius of the light source, NA is the numerical aperture, n is the refractive index of the tissue (1.36 for gray matter), and S is the scatter coefficient per unit thickness (z).

The calculation of time required by the storage capacitors to be able to have enough energy to illuminate the LED with respect to the number of cycles (of ultrasound frequency) is formulated as [8]:

$$n_{cycle_{charge}} = \left\lceil -\frac{V_{g_{par}} C_{cap_{par}}}{\Delta Q_{par}} \ln\left(1 - \sqrt{\frac{2E_{max_{par}}}{C_{cap} V_{g_{par}}^2}}\right)\right\rceil. \tag{9}$$

Meanwhile for illuminating the LED which is related to storage capacitor discharging, the required time with respect to the number of cycle is calculated using the series circuitry, and is represented as follows:

$$n_{cycle_{discharge}} = \left\lceil -\frac{V_{g_{ser}} C_{cap_{ser}}}{\Delta Q_{ser}} \ln\left(\sqrt{\frac{2E_{max_{ser}}}{C_{cap} V_{g_{ser}}^2}}\right)\right\rceil, \tag{10}$$

where E_{max} is the maximum electrical energy that can be stored in the storage circuit.

Furthermore, the voltage value during the charging and discharging process can be calculated based on the approach in [8], and is represented as follows:

$$V_{cap_{charge}}(n_{cycle}) = V_{g_{par}}\left(1 - e^{-\frac{n_{cycle_{par}}\Delta Q_{par}}{V_{g_{par}}C_{cap_{par}}}}\right), \quad (11)$$

$$V_{cap_{discharge}}(n_{cycle}) = V_{g_{ser}}e^{-\frac{n_{cycle_{ser}}\Delta Q_{ser}}{V_{g_{ser}}C_{cap_{ser}}}}. \quad (12)$$

In Eq. (11) and (12), subscript *par* and *ser* indicate the parallel and series connection of the storage capacitors, respectively.

Lastly, since we want to be able to invoke specific wi-opt neural dust to stimulate certain neurons, an addressing mechanism is required. In order to enable frequency selective lighting of the LEDs, a frequency filter switch can be incorporated into the circuit. The switch is a logical 'AND' gate that decides if the energy storage in the capacitor will lead to the discharging process of the LED. In this case, the concept of VOX (Voice Operated Switch) can be applicable.

IV. Simulations

TABLE I
Simulation Parameters

Parameter	Value [Unit]	Description
Neural Dust Density	0.024 to 1.2 [$/cm^3$]	Randomly scattered
Frequency	500 to 3M [Hz]	Ultrasound freq
Depth Radius	2 to 60 [mm]	Into the brain
Interfiring period	6 [ms]	Mean (exponential dist)
Data sample	10,000	Random data
Nanowire surface area	10^4 to 2×10^4 [μm^2]	Energy harvester

The wi-opt neural dust are simulated to investigate its optical behaviour when interfaced to cells as well as the behaviors of the device with respect to its charging and discharging capabilities to light up the LED. The parameters used for the simulations are presented in Table I.

A. Optical Light Behavior in Brain Tissue

Since the light source is embedded in the brain tissue, the light intensity is attenuated as it propagates through the tissue according to the attenuation coefficient of the medium. The optical power produced by the LED depends on the applied current percentage [13]. As the optical power level lessened by distance, the placement of the wi-opt neural dust has to consider the optimal position with regard to the optogenetic construct.

Monte Carlo simulations [15] and the Kubelka-Munk model [16] are often used to analyse light propagation in optogenetics field. In this work, we simulate the light propagation in human brain tissue using COMSOL Multiphysics software with Helmholtz model representation. The light transport model with Finite Element Method in COMSOL simulation includes the geometry and optical properties of the materials such as scattering and absorption. The model solves the fluence rate (light intensity) u or $\Phi(r,t)$, given the diffusion coefficient c or $D(r,t)$, absorption coefficient a or μ_a, and source term f or $S(r,t)$ according to the following Helmholtz equation:

$$\begin{aligned} -\nabla D(r,t)\nabla^2\Phi(r,t) + \mu_a\Phi(r,t) &= S(r,t) \\ \nabla(-c\nabla u) + au &= f. \end{aligned} \quad (13)$$

In our scenario, the LED is modeled as an ellipsoid, whereas the neuron cells and propagation medium as spheres. The absorption coefficients of LED, neuron cells, and brain tissue are set to 0, $0.36/mm$, and $0.014/mm$, respectively [15]. The diameters of LED and brain tissue model are $\approx 100\mu m$ and $500\mu m$, while we set $100\mu m$ diameter for single neuron cell and various diameters for more than one neuron cell model. The frequency domain study is chosen for wavelength of 470 nm which corresponds to blue light.

Fig.4(a) shows the light intensity generated by the light source radiated by half of the ellipsoid surface. Close to the source, the light intensity is high depicted by the red color. When we add the neuron cell model with the distance of $10\mu m$ from the light source, the intensity pattern changes due to different absorption coefficient of the materials. This phenomenon is shown in Fig.4(b). We also investigate the intensity pattern for the situation similar to the brain environment where there are more than one neuron cell close to each other. The distance range is between 10-20 μm by LED vicinity. Therefore, we add several neuron cells with the same optical properties but different sizes and distances from the light source. Fig.4(c) shows the light intensity pattern affected by multiple neuron cells.

From the simulation, it can be seen that distance and cells affect the attenuation of light propagation. As a result, the narrower pattern is formed as the number of surrounding neuron cells increases. This can be beneficial as one wi-opt neural dust might excite several optogenetic constructs if desired. On the other hand, it will create unwanted effects when excitation of undesired neuron occurs.

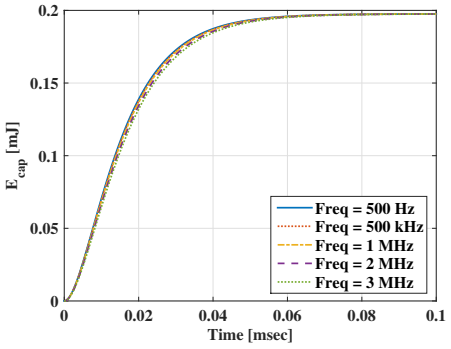

Fig. 5. Illustration of storage energy as a function of time with frequency variation where the neural dust mote is 2 mm deep into the brain during charging process.

B. Energy and Power Evaluation

In order to figure out the operational characteristics of a single wi-opt neural dust, it is important to evaluate the charging

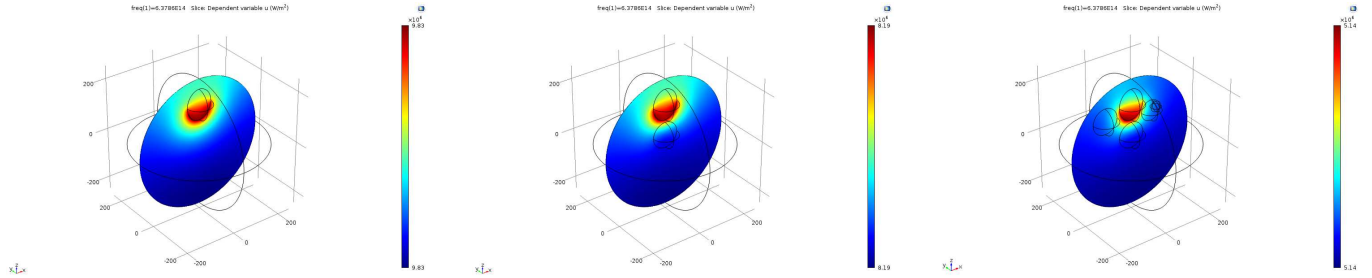

(a) Wi-opt neural dust LED light emission model (b) LED light emission on a single neuron cell. (c) LED light propagation surrounded by several neuron cells.

Fig. 4. COMSOL multiphysics simulation of the LED light propagation behaviour within the brain tissue.

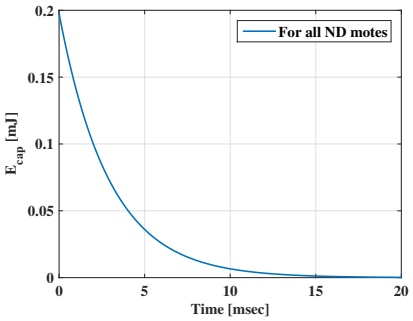

Fig. 6. Illustration of the storage energy as a function of time where the neural dust mote is 2 mm deep into the brain during discharging process.

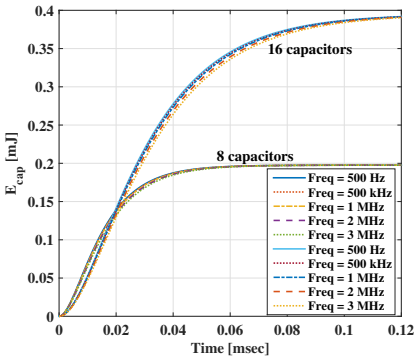

Fig. 7. Illustration of storage energy as a function of time with frequency variation where the neural dust mote is 2 mm deep into the brain during charging process.

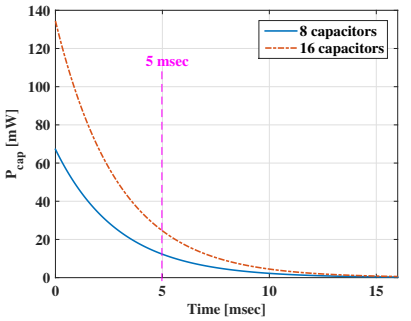

Fig. 8. Illustration of the capacitor power as a function of time where the neural dust mote is 2 mm deep into the brain during discharging process. The 5 msec limit is the minimum duration threshold required by the LED to emit light in order to successfully stimulate the neuron.

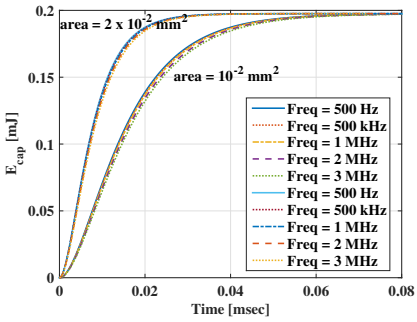

Fig. 9. Illustration of storage energy as a function of time for various frequencies and two different nanowire surface area.

and the discharging duration of the storage capacitors. These factors are affected mainly by the depth of the device planted into the brain and the frequency of the ultrasonic waves emitted from the sub-dura transceiver, while the constant intrinsic values of the storage capacitors are calculated based on the energy harvester and light source component. Considering the ontogenetic requirements for neuron stimulation, the circuit model explained in Sec.III has to be able to illuminate the LED for at least 5 msec duration [17]. In our simulations, each cycle utilizes 10 thousand random values for neuron sequence firing. The neuron inter-firing period is based on exponential distribution as their sequences can be represented as a poisson process (Rate as a Spike Count and Fano Factor) [18]. Fig. 5 presents the amount of stored energy with respect to time. Although higher frequencies suffer from higher attenuation within the brain tissue, this difference is very small in terms of the amount of energy stored with respect to time, as shown in Fig. 5. This also means that using different frequencies for the addressing mechanism will not come at a cost of variations in the charging durations. This factor must also be included in design consideration, especially when selective frequency is required to invoke specific wi-opt neural devices as well as the design of the sub-dura transceiver. Fig. 6 shows the graph

of the energy discharging of the capacitor storage. As shown in the discharging plot, the period to release the energy goes beyond the minimum 5 msec duration, ensuring that sufficient light intensity is applied to the neurons. Comparing Fig. 5 and Fig. 6, there is significant gap in time. The reason behind this is because the parallel and series capacitor connections during charging and discharging process. This configuration affects the electrical properties of the storage circuit, such as the capacitance value and the voltage value.

Fig. 7 present the results when different quantity of capacitors are used for the devices. Intuitively, we can see that an increase in the number of capacitors will definitely increase the quantity of energy stored, but comes at a cost of longer charging durations. This also means that higher number of ultrasound frequency cycles are required. The benefit of this configuration is that the device can maintain a certain amount of energy to stimulate neuron with short inter-firing periods, provided that a pausing process can be incorporated into the circuit. Fig. 8 presents the amount of energy discharged and compares between the different number of capacitors. For both configurations we can see that the discharging process provides sufficient amount of power and within the 5msec limit needed to stimulate the neuron. Since the charging process is reliant on vibration of the piezoelectric nanowires, Fig. 9 presents the results for variations in the area of the nanowire. There is no difference in the amount of energy charged when there are variations in the ultrasonic frequency. However, we can observe that the quantity of energy produced is increased when the area is doubled.

V. Conclusions

The increased attention towards Deep Brain Stimulation has attracted researchers to search for innovative solutions that can enable long-term deployment as well as design of miniaturised devices that can self-generate power. The emergence of optogenetics has provided a new approach for precise stimulation at the single neuron level. In this paper, we propose the wi-opt neural dust that is constructed from nanoscale components and can be embedded into the cortex of the brain. A thorough description of the circuitry as well as the components are presented, including mechanisms of generating power through ultrasonic wave vibrations. The paper presented simulation results on the behaviour of optical light transmission and its effect on the brain tissue, as well as the energy performance of the device based on variations of ultrasonic frequencies and circuitry devices (e.g. capacitors and piezoelectric nanowire area). The positive results from our simulation study has demonstrated the feasibility of using the wi-opt neural dust for long term deployments in the brain in order to stimulate neurons and provide new approaches for treating neurological diseases so that this study motivates future work in this direction.

Acknowledgment

This work is supported by the Academy of Finland FiDiPro (Finnish Distinguished Professor) program, for the project ”Nanocommunication Networks”, 2012-2016, and the Finnish Academy Research Fellow program under project no. 284531. This work has also been supported by the European Union Horizon 2020 CIRCLE project under the grant agreement No. 665564. This publication has also emanated from research supported in part by a research grant from Science Foundation Ireland (SFI) and is co-funded under the European Regional Development Fund under Grant Number 13/RC/2077. This work was also supported by the U.S. National Science Foundation (NSF) under Grants No. CBET-1445934 and CBET-1555720.

References

[1] X. Han. In vivo application of optogenetics for neural circuit analysis. *ACS chemical neuroscience*, 3(8):577–584, 2012.

[2] D. Seo, J. M. Carmena, J. M. Rabaey, E. Alon, and M. M. Maharbiz. Neural dust: An ultrasonic, low power solution for chronic brain-machine interfaces. *arXiv preprint arXiv:1307.2196*, 2013.

[3] V. B. Mountcastle. *Perceptual neuroscience: the cerebral cortex*. Harvard University Press, 1998.

[4] S. Song, A. Kim, and B. Ziaie. Omni-directional ultrasonic powering for millimeter-scale implantable devices. 2015.

[5] R. J. Przybyla, S. E. Shelton, A. Guedes, I. Izyumin, M. H. Kline, D. Horsley, B. E. Boser, et al. In-air rangefinding with an aln piezoelectric micromachined ultrasound transducer. *Sensors Journal, IEEE*, 11(11):2690–2697, 2011.

[6] M. Kim, J. Kim, and W. Cao. Electromechanical coupling coefficient of an ultrasonic array element. *Journal of applied physics*, 99(7):074102, 2006.

[7] P. R. Hoskins, K. Martin, and A. Thrush. *Diagnostic ultrasound: physics and equipment*. Cambridge University Press, 2010.

[8] J. M. Jornet and I. F. Akyildiz. Joint energy harvesting and communication analysis for perpetual wireless nanosensor networks in the terahertz band. *Nanotechnology, IEEE Transactions on*, 11(3):570–580, 2012.

[9] M. Beidaghi and C. Wang. Micro-supercapacitors based on interdigital electrodes of reduced graphene oxide and carbon nanotube composites with ultrahigh power handling performance. *Advanced Functional Materials*, 22(21):4501–4510, 2012.

[10] G. Nagel, T. Szellas, W. Huhn, S. Kateriya, N. Adeishvili, P. Berthold, D. Ollig, P. Hegemann, and E. Bamberg. Channelrhodopsin-2, a directly light-gated cation-selective membrane channel. *Proceedings of the National Academy of Sciences*, 100(24):13940–13945, 2003.

[11] T.-i. Kim, J. G. McCall, Y. H. Jung, X. Huang, E. R. Siuda, Y. Li, J. Song, Y. M. Song, H. A. Pao, R.-H. Kim, et al. Injectable, cellular-scale optoelectronics with applications for wireless optogenetics. *Science*, 340(6129):211–216, 2013.

[12] Cree Inc. *Direct Attach DA2432^{TM} LEDs*, 2013. Rev A.

[13] M. A. Rossi, V. Go, T. Murphy, Q. Fu, J. Morizio, and H. H. Yin. A wirelessly controlled implantable led system for deep brain optogenetic stimulation. *Frontiers in integrative neuroscience*, 9, 2015.

[14] A. M. Aravanis, L.-P. Wang, F. Zhang, L. A. Meltzer, M. Z. Mogri, M. B. Schneider, and K. Deisseroth. An optical neural interface: in vivo control of rodent motor cortex with integrated fiberoptic and optogenetic technology. *Journal of neural engineering*, 4(3):S143, 2007.

[15] Z. Wang, L. Wang, Y. Zhang, and X. Chen. Monte carlo simulation of light propagation in human tissue models. In *2009 3rd International Conference on Bioinformatics and Biomedical Engineering*, pages 1–4. IEEE, 2009.

[16] G. Yona, N. Meitav, I. Kahn, and S. Shoham. Realistic numerical and analytical modeling of light scattering in brain tissue for optogenetic applications. *eneuro*, pages ENEURO–0059, 2016.

[17] E. S. Boyden, F. Zhang, E. Bamberg, G. Nagel, and K. Deisseroth. Millisecond-timescale, genetically targeted optical control of neural activity. *Nature neuroscience*, 8(9):1263–1268, 2005.

[18] W. Gerstner, W. M. Kistler, R. Naud, and L. Paninski. *Neuronal dynamics: From single neurons to networks and models of cognition*. Cambridge University Press, 2014.